Soot Oxidation Kinetics of Different Ceria Nanoparticle Catalysts

ARTICLE · JULY 2015

DOI: 10.1007/s40825-015-0021-z

3 AUTHORS, INCLUDING:

Georgia Kastrinaki
The Centre for Research and Technology, H…
6 PUBLICATIONS **13** CITATIONS
SEE PROFILE

Souzana Lorentzou
The Centre for Research and Technology, H…
39 PUBLICATIONS **228** CITATIONS
SEE PROFILE

Emiss. Control Sci. Technol. (2015) 1:247–253
DOI 10.1007/s40825-015-0021-z

Soot Oxidation Kinetics of Different Ceria Nanoparticle Catalysts

Georgia Kastrinaki[1] · **Souzana Lorentzou**[1] · **Athanasios G. Konstandopoulos**[1,2]

Received: 14 June 2015 / Revised: 16 June 2015 / Accepted: 17 June 2015 / Published online: 8 July 2015

Abstract Catalysts for direct soot oxidation in catalyzed diesel particulate filters (CDPFs) consist typically of various mixed oxide compositions (frequently with CeO_2 as the dominant component) that assist soot oxidation by enhancing the supply of oxygen from the catalyst to the soot. Apart from the composition, the material morphological characteristics may also contribute to the catalytic activity and this is the motivation for the present study. Different CeO_2 nanoparticle catalysts have been obtained employing aerosol-based synthesis (ABS) and sol–gel methods. The obtained catalyst particles have been characterized with respect to their physical and morphological properties as well as with respect to their catalytic soot oxidation activity. The results have been analyzed with the aid of a multi-population kinetics model where soot is found to consist of three fractions reacting with different activation energies, namely 120, 180, and 240 kJ/mol. The occurrence of these three fractions is attributed to the formation of distinct families of surface oxygen complexes (SOCs) on the carbon surface which are subsequently gasified and hence cause soot oxidation, in agreement with accepted mechanisms of soot oxidation in the literature. The CeO_2 nanoparticles oxidize catalytically all three fractions of soot, but with different "enhancement factors," while the activation energies during catalytic oxidation remain the same. A comparison of the catalytic pre-exponentials to those of plain soot shows, in most cases, enhancements, which for some catalysts, can be up to ~4.5, 6.5, and 2 times larger than those of plain soot, reflecting the relative capacity of the catalyst to generate more of the respective SOCs. The developed approach provides a more detailed but tractable way to describe soot oxidation (plain and catalytic), which can be readily incorporated into simulations of actual emission control systems to increase their reliability.

Keywords Catalytic soot oxidation · Ceria · Nanoparticles · Kinetics model

Abbreviations

CDPF	Catalytic diesel particulate filter
ABS	Aerosol-based synthesis
XRD	X-ray diffraction
SOC	Surface oxygen complex
SEM	Scanning electron microscopy
TGA	Thermo-gravimetric analysis
BET	Brunauer–Emmett–Teller
BJH	Barrett–Joyner–Halenda

1 Introduction

Current emission control requirements for diesel engines have resulted in the widespread introduction of diesel particulate filters (DPFs) that efficiently collect soot particles from the exhaust and subsequently oxidize them in a process known as regeneration. Direct oxidation of soot can be accelerated by incorporation of catalysts (typically transition and rare earth metals oxides) in the DPF (a so-called catalytic DPF, CDPF) at typically a lower temperature than that required for pure thermal oxidation (>650 °C) [1].

✉ Athanasios G. Konstandopoulos
agk@cperi.certh.gr

[1] Aerosol and Particle Technology Laboratory, CERTH/CPERI, P.O. Box 60361, Thermi, 57001 Thessaloniki, Greece

[2] Department of Chemical Engineering, Aristotle University, PO. Box 1517, 54006 Thessaloniki, Greece

One of the most common components of such catalysts used in such applications, is cerium oxide, CeO_2. It has been widely used for a number of years in three-way catalysts for spark-ignition engines and as a fuel additive in the case of diesel engines [2]. In a CDPF, cerium oxide is usually incorporated in a doped/mixed oxide form to enhance its oxygen storage capacity and hence capability for direct soot oxidation, as well as take advantage of the stabilized structural characteristics of the doped/mixed oxide [3-11].

The problem of soot-catalyst contact was recognized from the beginning of diesel particulate control development [12] as a barrier for active catalytic filter development, and it has become widely appreciated with the introduction of "loose" contact studies [13] of powdered soot-catalyst mixtures (as opposed to a well ground "tight" contact mixture), see also [4].

It is also interesting, however, to point out that the intrinsic soot oxidation activity (under conditions of so-called tight contact [4]) may depend on morphological and structural characteristic of the catalytic materials [5]. The fact that no well-defined analysis exists to separate and classify the relative importance of these factors (without any subjective references to loose vs tight contact) motivates the present work. The present study is an effort to investigate such phenomena, employing simple, well-controlled experiments of catalytic soot oxidation in close combination with a general multi-population model of soot oxidation e.g. [14, 17] for data analysis.

In the current work, two groups of cerium oxide materials were synthesized in order to study the effect of different morphological and structural characteristics in catalytic soot oxidation. The first group of materials was cerium oxide particles synthesized by aerosol-based synthesis (ABS) and the second one by sol–gel synthesis techniques allowing to sample a wide space of different morphological properties: crystallite size, mean particle diameter, and surface area. The materials were also characterized by x-ray diffraction (XRD) for the determination of their crystal phases and by Brunauer–Emmett–Teller (BET) for their surface area and pore structure. In addition, the particles were also studied with transmission electron microscopy (TEM) for a finer morphological characterization.

Mixtures of the aforementioned catalysts with a quantity of soot were studied by thermo-gravimetric analysis (TGA) regarding their catalytic oxidation activity. The reaction rate and the kinetic model parameters are then calculated.

2 Experimental

2.1 Materials Synthesis Routes

As the focus of the present paper is the analysis of the catalytic activity of "same chemistry" catalysts, namely CeO_2, the catalyst preparation is only briefly outlined and details of the different synthesis methods will be presented in a future paper. ABS is a synthesis method during which a precursor solution is atomized into fine droplets (~2-μm mean diameter) which pass through a heated tube reactor, where evaporation of the solvent, precipitation of the solutes, and reaction in the solid phase take place at the droplet level. By modifying the different parameters of the synthesis conditions that affect the precipitation and assembling reactions that take place on the droplet level (e.g., the heated wall reactor temperature and gas flow), different particle morphologies can be achieved. The produced particles are collected on a quartz fiber filter at the reactor exit [15]. The ABS method for the cerium oxide particles employ aqueous solutions of cerium precursors (typically inorganic salts) together with other additives (typically surfactants and/or pore formers and/or binders). It is known that the precursor concentration affects the crystallite size of the synthesized particles, their diameter, and consequently, their surface area [16]. The sol–gel solutions after thermal treatment for 2 days at 180 °C are calcined at 450 °C for 5 h under air and a catalytic powder is recovered.

2.2 Methods

2.2.1 Soot

A flame-generated carbon black (Statex, N330) was employed as a reference soot to warrant absence of inorganic ashes which could interfere with the ceria materials catalytic

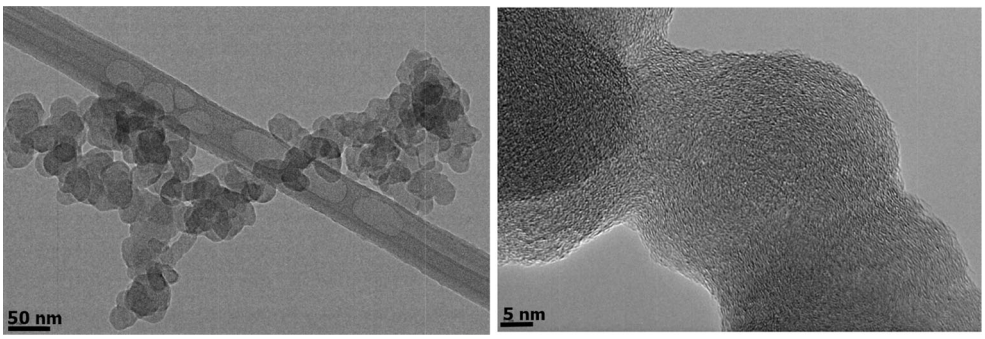

Fig. 1 TEM images of the soot employed in the study

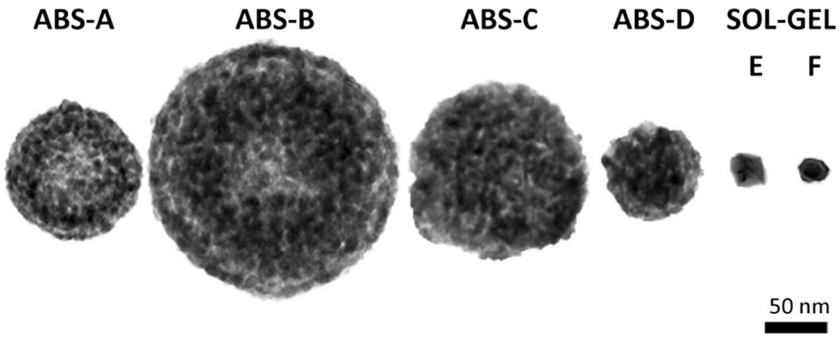

Fig. 2 TEM images of all synthesized particles (mean particle size of each sample)

activity. The carbon black aggregates are composed of near-spherical primary particles (~26 nm) and have a 74.2 m^2/g surface area (Fig. 1).

2.2.2 Ceria Catalysts

The produced ceria particles (shown in Fig. 2) were characterized by x-ray diffraction (Siemens D500/501) for their crystal phase and their crystallite size was calculated by employing the Scherrer equation at the main peak of cerianite (at 29 ° for both commercial and in-house materials). High-resolution transmission electron microscopy (JEOL JEM 2010) was used for the characterization of the synthesized materials. BET method measurements were performed by an Autosorb-1 instrument at specific outgassing temperature of 150 °C for the calculation of the BET surface area and pore size from the Barrett–Joyner–Halenda (BJH) adsorption/desorption cumulative surface area of pores and average pore width, respectively. The evaluation of the catalytic activity of the produced powders, with respect to soot oxidation, was conducted by thermo-gravimetric analysis. Mixtures of the produced oxides with soot were ground together in a mortar at a ratio of 2:1 on a mass basis. The mixtures were subsequently placed in a thermo-gravimetric analyzer (PerkinElmer Pyris-6 TGA) and heated under 20 % O_2 in N_2 with a temperature increase rate of 3 °C/min from 150 up to 700 °C.

3 Results

3.1 Morphological characterization

Table 1 depicts the structural characteristics—such as mean particle diameter, crystallite size, surface area, and pore size—of the synthesized materials. The mean particle size is calculated from the cumulative size analysis of many particles from multiple TEM images.

The crystallite size for all the materials is calculated by applying the Scherrer equation to the XRD data of Fig. 3 and, in particular, to peak of the main phase of cubic-fluorite cerium oxide in the (111) orientation. The surface areas and pore sizes are evaluated by the BET method. For the sol–gel samples, no pore size could be determined and the samples may be assumed to be fairly dense. The comparison of the particle size of the ABS and sol–gel particles reveals one order of magnitude lower sizes for the latter. The crystallite size of the samples varies from 9 to 29 nm, while the surface area of the ABS samples varies from 8 to 59 m^2/g. The porosity was calculated from the crystallite size and the pore size for a packing of spherical particles.

The comparative XRD (Fig. 3) demonstrates the cerianite (CeO_2) peaks that are exhibited by all of the synthesized samples. In addition, all samples exhibit high crystallinity as evidenced by the sharpness of the relative XRD peaks, while the wider (111) peak of material A is a manifestation of the small crystallite size of the material.

Table 1 Morphological characteristics of CeO_2 catalysts that were employed in this study

Sample	Synthesis method	Mean particle size (nm)	Crystallite size (nm)	Surface area (m^2/g)	Pore size (nm)	Porosity (–)
A	ABS	87	9	59	12.4	0.674
B	ABS	172	25	37	10.5	0.387
C	ABS	138	18	35	20.7	0.633
D	ABS	77	25	8	13.7	0.451
E	Sol–gel	30	29	5	–	–
F	Sol–gel	21	18	12	–	–

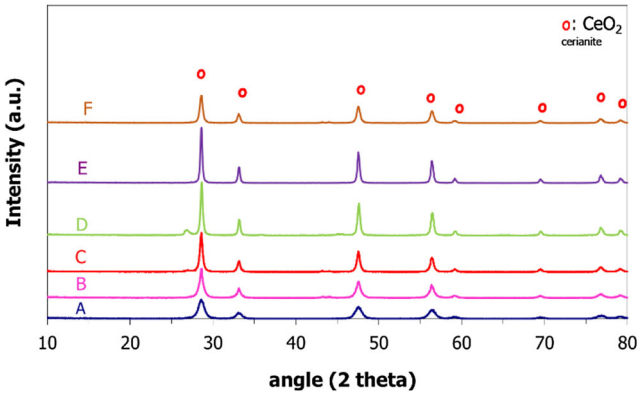

Fig. 3 X-ray diffraction diagrams of the samples

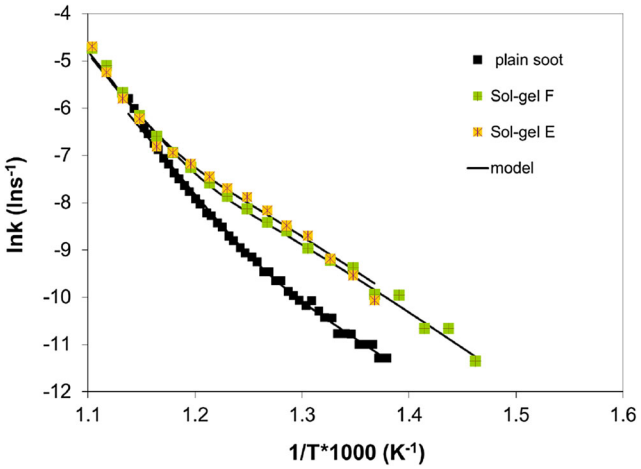

Fig. 5 Arrhenius plot for the sol–gel ceria samples

3.2 Catalytic Soot Oxidation

Figure 4 depicts the soot oxidation rate as a function of temperature for all catalyst samples. It is observed that ABS synthesized materials exhibit lower soot oxidation temperature compared to the sol–gel samples. Given the same chemical composition of the samples, these differences need to be traced to the different morphological and structural particle characteristics of the synthesized catalysts.

The oxidation of soot with catalytic particles are recast in the form of Arrhenius plots, where the pseudo-first-order instantaneous rate $k=(1/m)\ dm/dt\ (s^{-1})$ is plotted as a function of $1000/T\ (K^{-1})$. Interestingly enough, as shown in Figs. 5 and 6, it is evident that although the overall behavior of the soot oxidation is non-Arrhenius, there exist multiple linear regions in the plot, similar to our earlier observations [17].

The origin of different linear segments in the Arrhenius plots is a manifestation of multiple types of soot reacting and deserves further discussion. In our earlier work [17], such behavior for plain soot was attributed to distinct populations of soot as, e.g., indicated by the presence of ordered and disordered types of carbon structures in soot particle Raman spectra, as well as due to the frequent existence of an (ordered) core—(disordered) shell structure of the soot primary particles. In this essentially, phenomenological description, different activation energies (different slopes in the Arrhenius plot) were attributed to the different "types of soot" while different oxidation rates for "same-slope soot types" were attributed to different pre-exponential coefficients, implicitly assumed to be different for different types of soot, e.g., those produced at varying engine conditions. Similar behavior (multiple linear segments in Arrhenius plots) for soot oxidation in catalyzed particulate filters was attributed to the occurrence of various contact states among the soot and catalyst sites (an extension of the so-called two-layer model of a catalytic coating for soot oxidation). However, Fig. 6 demonstrates that even under conditions of so-called tight contact, such behavior can be observed. Considering that the mechanism of soot oxidation (thermal and catalytic) involves the creation and subsequent "gasification" of surface oxygen complexes (SOCs), see e.g., [18] and cited references therein, a more complete approach to the problem needs to examine soot oxidation from the perspective of being/becoming a "host" for SOCs and how catalysts such as CeO_2 (which to this level of description, act

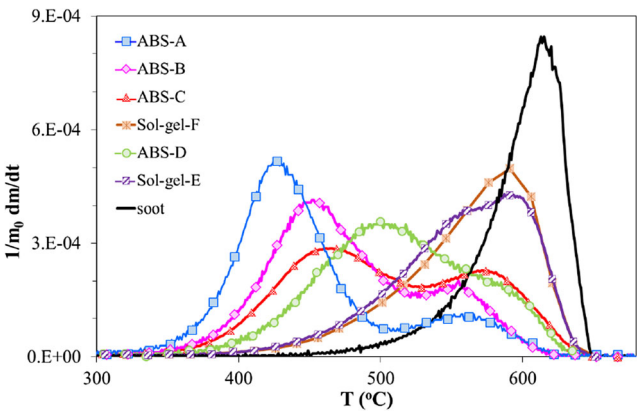

Fig. 4 Soot oxidation activity (expressed as a normalized reaction rate in s^{-1}) of the CeO_2 catalysts

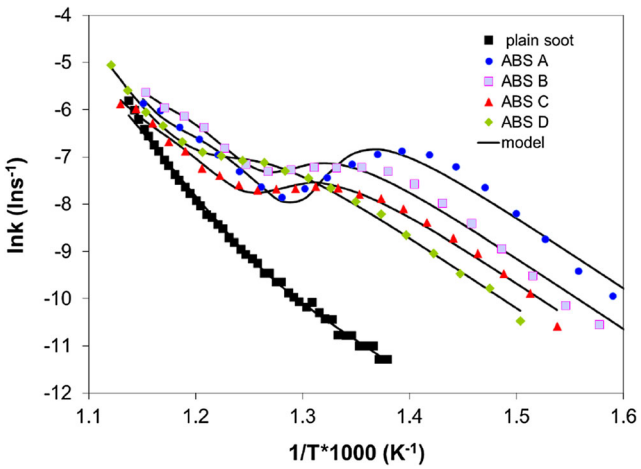

Fig. 6 Arrhenius plot for the ABS samples

as oxygen pumps facilitating the creation of SOCs) enhance this ability. In this description, we may consider a soot primary particle to exhibit a mixture of different morphological features (i.e., various types of order/disorder) which can be, to various degrees, favorable hosts for particular types of SOCs. Taking into account that there are various SOCs which may be "anchored" on the soot surface with one (e.g., carboxyl, carbonyl), two (lactone, quinone, ether), or three (e.g., phenol) "bonds to the surface" (see e.g., [18] for schematics) and considering that the soot oxidation activation energy is essentially "spent" to "break the SOC bonds" from the carbon surface, we can now enhance our previous phenomenological description with some more physicochemical elements.

At this point, it is useful to summarize the description discussed earlier. We consider soot reactivity to be essentially determined by the reactivity of its primary particle microstructure and the overall reactivity can be determined by a mixture (additive) approach of different oxidation paths. The soot microstructure can be favorable or less favorable host (i.e., exhibiting higher or lower pre-exponential factor) to various types of SOCs which may be subsequently be driven off the surface ("gasified") upon breaking of the different bonds that hold them on the surface (hence the origin of different activation energies in the Arrhenius plot). Adding a catalyst into the picture can enhance the formation of particular SOCs by supplying oxygen to the carbon surface (increasing thus the pre-exponential factor of a particular SOC gasification path but not changing its activation energy). The extent to which this is possible is determined by the soot-catalyst proximity; therefore, the pre-exponential factor includes this dependence by a multiplicative constant, which needs to be determined by varying the soot-catalyst ratio, see e.g., [19] for a similar determination for soot-fuel borne catalyst system.

A multi-population kinetics model can be then formulated for the analysis of the data in Figs. 5 and 6 as follows. The total soot mass is decomposed into several fractions, each one reacting with its own reaction rate constant, following first-order kinetics:

$$\frac{dm_i}{dt} = -k_i m_i \qquad ([1])$$

for $i=1$ to n, where m_i is the soot mass in fraction i, k_i is the corresponding rate (ordered in decreasing order as i increases). The actual form of the reaction rate constant is taken to be $k_i=A_i[O_2]T\exp(-E_i/RT)$, i.e., that of a modified Arrhenius type. For simplicity in the present exposition, the pre-exponential constant is assumed to include also the dependence on oxygen concentration (which for the experimental data is a constant); however, a simpler Arrhenius form and explicit inclusion of dependence on the oxygen concentration with a power as well as on the surface area evolution as a function of conversion (e.g., for a shrinking core or shrinking density oxidation mode) can be straightforwardly included without any limitation. The initial amount of soot in each fraction m_{i0} is written in terms of the mass fractions φ_{i0}, as $m_{i0}=\varphi_{i0}m_0$, where m_0 is the initial sample mass and $\sum\varphi_{i0}=1$. Imposing a known temperature evolution, i.e., the experimental temperature profile $T(t)=T_0+\lambda t$ (λ is the temperature ramp), we can then integrate Eq. (1) forward and fit the experimental data employing a non-linear fitting routine.

The plain soot (uncatalyzed) oxidation data in Figs. 5 and 6 are fitted with a three-population kinetic model indicated by the solid lines designated as "model." The three soot fractions φ_{i0} obtained, the activation energies E_i, and pre-exponential factors k_i for each fraction are shown in Table 2. The data with the catalytic materials are also fitted with the same set of activation energies, allowing the soot fractions and pre-exponential factors to be determined.

By cross-referencing the data of Table 1 to the data of Table 2, it is possible to arrive at some general criteria regarding how the morphological and structural characteristics of CeO_2 catalysts affect their catalytic soot oxidation activity. The most active sample (A) appears to have the largest surface area, smallest crystallite size, largest porosity, second-smallest pore size, and an intermediate particle size compared to all other samples. Presumably, all but the last are factors that affect the generation of "active oxygen" which subsequently forms different types of SOCs and in varying numbers on the soot surface, while the last factor (particle size) determines "the effectiveness of the contact" of the soot primary particles in proximity to the catalyst particle. It is clear from the data in Table 2 that there is no monotonic relation of catalytic activity

Table 2 Kinetic parameters calculated for all samples

Sample	Activation energy (kJ/mol)			Pre-exponential factor (1/sK¯)			Soot fraction (−)		
	E_1	E_2	E_3	k_1	k_2	k_3	φ_{10}	φ_{20}	φ_{30}
Plain soot	240	180	120	5.0E+08	1.0E+5	257	0.651	0.33	0.020
A				9.2E+08	6.6E+05	1177	0.051	0.124	0.825
B				1.0E+09	5.9E+05	567	0.042	0.235	0.724
C				4.6E+08	3.2E+05	413	0.129	0.292	0.579
D				7.6E+08	4.6E+05	203	0.159	0.155	0.686
E				5.3E+08	1.8E+05	88	0.360	0.330	0.310
F				5.7E+08	1.8E+05	114	0.445	0.330	0.225

to catalyst particle size. The detailed contact arrangements of soot aggregates ground together in the mortar with catalyst particles are the subject of an ongoing investigation, and it will be reported in a future publication.

4 Conclusions

An accurate description of soot reactivity requires a multi-population kinetics approach. Based on our current and past research, we can identify three populations (fractions) of soot that are reacting with activation energies 120, 180, and 240 kJ/mol (all activation energies fall within the range of carbon oxidation activation energies, see e.g., [1, 4, 12, 13]). The activation energies are found to differ in multiples of 60 kJ/mol for all samples and these measurements are also consistent with several other measurements in our laboratory. These differences in the activation energies most likely reflect the differences in SOCs that are favored to be formed on each soot fraction microstructure. It is tempting therefore to hypothesize that there are at least three families of SOCs each with different bond configurations on the carbon surface, say with one, two, and three bonds and to drive them off the carbon surface requires activation energies of 120, 180, and 240 kJ/mol, respectively. Interestingly enough, the activation energies of 120 and 180 kJ/mol have been also observed in studies of diesel soot oxidation in diesel particulate filters [17].

Ceria-nanoparticles oxidize catalytically all three fractions of soot, but with different "enhancement factors." The activation energies during catalytic oxidation remain the same (120, 180, and 240 kJ/mol). A comparison in Table 2 of the catalytic pre-exponentials to those of plain soot shows, in most cases, enhancements which, for some catalysts, can be up to ~4.5, 6.5, and 2 times larger than those of plain soot, reflecting the relative capacity of the catalyst to generate more of the respective SOCs. Those few cases where the catalytic data show smaller pre-exponentials (for the most active 120 kJ/mol fraction) are interpreted as being due to the formation of lower amounts of the specific SOCs in the presence of the catalyst. It appears that the most active catalyst had an intermediate size, high surface area, small crystallite size, small pore size, and large porosity. However, the possibility of deriving a composite microstructural metric to correlate the kinetic data, although now closer to our reach, still remains a challenge for future research. The present study provides a more detailed but tractable way to describe soot oxidation (plain and catalytic) which is readily incorporated into the framework of particle filter simulations [20].

Acknowledgments We thank the European Commission for its support of this work through the APT-STEP Project (FP7-REGPOT-2012-CT2012-315871-APT-STEP), and the General Secretariat for Research and Technology for its support through the KRIPIS Project CERTH-SYNERGY and the CHORUS Clean Energy Cluster

References

1. Konstandopoulos A.G., Papaioannou E., Zarvalis D., Skopa S., Baltzopoulou P., Kladopoulou E., Kostoglou M, Lorentzou S.: Catalytic filter systems with direct and indirect soot oxidation activity. SAE Tech. Paper No. 2005-01-0670 (SP-1942) (2005)
2. Salvat O., Marez P., Belot G.: Passenger car serial application of a particulate filter system, on a common rail direct injection diesel engine PSA PEUGEOT CITROEN. SAE Tech. paper No. 2000-01-0473 (2000)
3. Lorentzou, S. Pagkoura, C. Zygogianni, A. Kastrinaki, G. Konstandopoulos, A.G.: Catalytic nano-structured materials for next generation diesel particulate filters. SAE Technical paper, 2008-01- 0417 (2008)
4. Van Setten, L., Makkee, M., Moulijn, J.S.: Science and technology of catalytic diesel particulate filters. Catal Rev **43**(4), 489–564 (2001)
5. Bensaid, S., Russo, N., Fino, D.: CeO_2-based catalysts with engineered morphologies for soot oxidation to enhance soot-catalyst contact. Nanoscale Res Lett **9**, 254 (2014)
6. Liang, X., Xiao, J., Chen, B., Li, Y.: Catalytically stable and active CeO_2 mesoporous spheres. Inorg Chem **49**, 8188–8190 (2010)
7. Bueno-López, A., Krishna, K., Makkee, M., Moulijn, J.A.: Active oxygen from CeO_2 and its role in catalysed soot oxidation. Catal Lett **99**(3–4), 203–205 (2005)
8. Aneggi, E., de Leitenburg, C., Trovarelli, A.: On the role of lattice/surface oxygen in ceria–zirconia catalysts for diesel soot combustion. Catal Today **181**, 108–115 (2012)
9. Aneggi, E., Wiater, D., de Leitenburg, C., Llorca, J., Trovarelli, A.: Shape-dependent activity of ceria in soot combustion. ACS Catal **4**, 172–181 (2014)
10. Aneggi, E., de Leitenburg, C., Llorca, J., Trovarelli, A.: Higher activity of diesel soot oxidation over polycrystalline ceria and ceria–zirconia solid solutions from more reactive surface planes. Catal Today **197**(10), 119–126 (2012)
11. Durgasri N. D, Vinodkumar T., Lin F., Alxneit I., Reddy B.M.: Gadolinium doped cerium oxide for soot oxidation: Influence of interfacial metal–support interactions. Applied Surface Science, 314 (2014)
12. Murphy M. J., Hillenbrand L. J., Trayser D. A., Wasser J. H.: Assessment of diesel particulate control–direct and catalytic oxidation. SAE Tech. Paper No. 810112 (1981)
13. Neeft, J.P.: Catalytic oxidation of soot; potential for the reduction of diesel particulate emissions, Ph.D. Thesis. Technical University of Delft, Netherlands (1995)
14. Konstandopoulos A.G., Kostoglou M., Lorentzou S.: The Micromechanics of Catalytic Soot Oxidation in Diesel Particulate Filters, SAE Tech. Paper No. 2012-01-1288, SP, 2325, 41–68 (2012)
15. Karadimitra, K., Papaioannou, E., Konstandopoulos, A.G.: Oxidation of diesel particulate in catalytic filters coated by aerosol spray pyrolysis. J Aerosol Sci **32**(1), 233–234 (2001)
16. Lorentzou, S., Kastrinaki, G., Pagkoura, C., Konstandopoulos, A.G.: Oxide nanoparticles for hydrogen production from water-splitting and catalytic oxidation of diesel exhaust emissions. Nanosci Nanotechnol Lett **3**(5), 697–704 (2011) **(8)**
17. Konstandopoulos, A.G., Kostoglou, M., Lorentzou, S., Vlachos, N.: Aspects of multifunctional diesel particulate filters and their efficient simulation. Catal Today **188**(1), 2–13 (2012)

18. Setiabudi A, Makkee M, Moulijn J A.: The role of NO_2 and O_2 in the accelerated combustion of soot in diesel exhaust gases, Applied Catalysis B: Environmental, (2004)
19. Konstandopoulos A.G., Kostoglou M., Lorentzou S., Pagkoura C., Papaioannou E., Ohno K., Ogyu K., Oya T.: Soot Oxidation Kinetics in Diesel Particulate Filters, SAE Tech. Paper, No. 2007-01-1129, SAE Trans. 116 (J. Fuels & Lubricants), pp. 173–181. (2007)
20. Konstandopoulos, A.G., Kostoglou, M., Vlachos, N., Kladopoulou, E.: Advances in the science and technology of diesel particulate filter simulation. Adv Chem Eng **33**, 213–275 (2007)